

Ultrastable phonon frequencies in α -quartz-type BPO_4 at high temperature

Cite as: Appl. Phys. Lett. **115**, 141902 (2019); <https://doi.org/10.1063/1.5111621>

Submitted: 29 May 2019 . Accepted: 13 September 2019 . Published Online: 30 September 2019

R. Le Parc,  E. Buixaderas, C. Levelut, P. Hermet, A. S. Pereira, O. Cambon, C. Rolland, P. Simon, and  J. Haines



View Online



Export Citation



CrossMark

ARTICLES YOU MAY BE INTERESTED IN

[Local elasticity and macroscopic plasticity in homogeneous and heterogeneous bulk metallic glasses](#)

Applied Physics Letters **115**, 141901 (2019); <https://doi.org/10.1063/1.5109220>

[Multiphonon resonant Raman scattering and the second-order Raman processes in the excitonic luminescence of ZnO](#)

Applied Physics Letters **115**, 142103 (2019); <https://doi.org/10.1063/1.5120879>

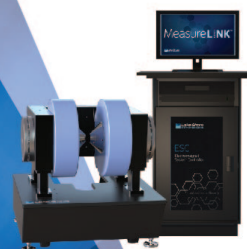
[A van der Waals epitaxial growth of ultrathin two-dimensional Sn film on graphene covered Cu\(111\) substrate](#)

Applied Physics Letters **115**, 141601 (2019); <https://doi.org/10.1063/1.5098037>

 **Measure Ready**
MCS-EMP Modular Characterization Systems

NEW

Multi-purpose platforms for
automated variable-field experiments



 **Lake Shore**
CRYOTRONICS

Find out more

AIP
Publishing

Ultrastable phonon frequencies in α -quartz-type BPO_4 at high temperature

Cite as: Appl. Phys. Lett. **115**, 141902 (2019); doi: [10.1063/1.5111621](https://doi.org/10.1063/1.5111621)

Submitted: 29 May 2019 · Accepted: 13 September 2019 ·

Published Online: 30 September 2019





View Online



Export Citation



CrossMark

R. Le Parc,¹ E. Buixaderas,^{2,3}  C. Levelut,¹ P. Hermet,⁴ A. S. Pereira,⁵ O. Cambon,⁴ C. Roiland,^{2,6} P. Simon,² and J. Haines^{4,a)} 

AFFILIATIONS

¹L2C, CNRS, Université de Montpellier, Montpellier, 34095 cedex, France

²CNRS, UPR 3079 CEMHTI, Université d'Orléans, 45071 cedex 2, Orléans, France

³Institute of Physics, Czech Academy of Sciences, 182 21 Prague 8, Czech Republic

⁴ICGM, CNRS, Université de Montpellier, ENSCM, Montpellier, 34095 cedex, France

⁵Instituto de Física and Escola de Engenharia, Universidade Federal do Rio Grande do Sul, 91501-970 Porto Alegre, Rio Grande do Sul, Brazil

⁶ISCR, CNRS, Université de Rennes 1, 35042 cedex, Rennes, France

^{a)}Author to whom correspondence should be addressed: Julien.Haines@umontpellier.fr

ABSTRACT

The Raman modes of α -quartz-type boron phosphate were found to be extremely stable in frequency over a large temperature range from 300–1000 K. In order to determine the origin of this behavior, the material was also studied at high pressure up to 6 GPa. Upon compression, a classical behavior was observed with mode Grüneisen parameters ranging from $-0.08(2)$ to $3.0(1)$. The present results indicate that the high temperature behavior in this material is an example of an unusual compensation effect between phonon–phonon interactions and implicit contributions due to thermal expansion. Phonon stability is of utmost importance for materials properties that are dependent on it such as dielectric and piezoelectric properties, for example. Boron phosphate belongs to the important class of α -quartz-type piezoelectric materials for which temperature stability is of primordial importance for resonator and sensor applications.

Published under license by AIP Publishing. <https://doi.org/10.1063/1.5111621>

α -Quartz and its homeotypes represent a major class of piezoelectric materials used in applications as resonators and oscillators. Particularly, in the case of space applications, the frequency stability is of major importance: the relative frequency shift must not exceed 10^{-9} per month. Until now, quartz oscillators have been thermally stabilized at 80°C to reach such a stability. Oscillators based on BPO_4 could be of higher stability without any thermal stabilization. In other applications, temperature stability is of primordial importance for the stability of resonators and also for applications as in, for example, high-temperature pressure sensors, microbalances, and field-test viscometers. α -quartz-type BPO_4 is the dense, metastable polymorph of cristobalite-type BPO_4 obtained by high-pressure-high temperature treatment.^{1–4} Due to the presence of electron-deficient boron, this material has particular bonding characteristics. BPO_4 exhibits the highest stability under high pressure of the α -quartz group of materials as it is stable to more than 50 GPa and it is highly incompressible with a bulk modulus of 92 GPa,⁴ which is almost three times that of α -quartz SiO_2 .⁵

Phonon frequencies in normal solids shift to lower values at high temperature due to phonon anharmonicity.^{6–10} Explicit contributions (phonon–phonon interactions or Umklapp term) correspond to increased amplitude of vibration at high temperature. Implicit contributions to the phonon frequency shift arise as bond lengths increase due to thermal expansion effects. Phonon stability at high temperature is of great interest as the functional properties which depend on them (dielectrics, piezoelectricity...) will also exhibit high temperature stability.

In the present study, BPO_4 was investigated by Raman scattering at high temperature and at high pressure along with complementary density functional theory calculations in order to understand the unusual ultrastable optical phonon frequencies that were observed as a function of temperature.

α -quartz-type BPO_4 powder was prepared from the cristobalite form in a belt-type apparatus at 7.8 GPa and 1273 K as described previously.³ Raman spectra were obtained on a Jobin–Yvon T64000 spectrometer operating in triple subtractive mode

(three 1800 grooves/mm gratings) and equipped with a liquid nitrogen cooled CCD detector. The 514.532 nm line of an argon–krypton Coherent Innova 70 Spectrum laser was used for excitation. An Olympus confocal optical microscope was used to focus the laser into an $\sim 2\ \mu\text{m}$ sized spot on the sample. All experiments were performed in backscattering geometry. High-temperature Raman spectra were obtained using a Linkam TS 1500 heating stage with a type S Pt-10% Rh/Pt thermocouple to measure the temperature. In order to take into account thermal population effects, the spectra were fitted with damped harmonic oscillator functions which include the Bose–Einstein factor, as described previously;¹¹ this limits artifacts due to the baseline subtraction and the blackbody emission. High-pressure Raman measurements were also performed with a Jobin-Yvon T64000 confocal microRaman spectrometer in both simple (notch filter) and triple-monochromator configurations using a $50\times$ long distance microscope objective. The 514.532 nm line from a Coherent Argon ion laser was used for excitation. The experiments at high pressure were performed with an EasyLab Helios membrane diamond anvil cell. The ($120\ \mu\text{m}$) hole in the $70\ \mu\text{m}$ thick preindented stainless steel gasket was filled with the powdered BPO_4 , ruby spheres, and 16:4:1 methanol:ethanol: H_2O as a pressure transmitting medium. The pressure in the DAC was determined from the spectral shift of the ruby R_1 fluorescence line.¹²

The first-principles calculations were performed within density functional theory and the local density approximation¹³ using the ABINIT package.¹⁴ B($2s^2, 2p^1$), P($3s^2, 3p^3$), and O ($2s^2, 2p^4$)-electrons were treated as valence states. The wavefunction was expanded in plane waves up to a kinetic energy cutoff of 60 Ha. Integrals over the Brillouin zone were replaced by sums over a $8 \times 8 \times 4$ Monkhorst–Pack mesh of special k-points.¹⁵ Lattice parameters and atomic positions were fully relaxed using a Broyden–Fletcher–Goldfarb–Shanno algorithm until the maximum stresses and residual forces were less than 2×10^{-4} GPa and 2×10^{-6} Ha/Bohr, respectively. Our relaxed lattice parameters ($a = 4.422\ \text{\AA}$ and $c = 9.840\ \text{\AA}$) are in good agreement (relative error about -0.8%) with the experimental ones.³ The dynamical matrix at the zone center has been obtained using a linear response approach, and Raman spectra have been recorded according to Ref. 16. The first principles calculations were also performed as a function of pressure in order to determine the pressure dependence of the Raman mode frequencies.

Group theory predicts that the α -quartz homeotype BPO_4 (Trigonal $P3_121 D_3^4, Z = 3$) will exhibit 54 modes of vibration,

$$\Gamma = 8 A_1 + 10 A_2 + 18 E.$$

One A_2 and one pair of degenerate E modes are acoustic, and the remaining optical modes are

$$\Gamma = 8 A_1 + 9 A_2 + 17 E.$$

The 8 nondegenerate A_1 and 17 doubly degenerate E modes are predicted to be Raman active.

Due to some differences in sample orientation and in polarization conditions, unavoidable with such small samples as here (some hundreds of micrometer in the temperature experiments and even smaller in the DAC device), the room-conditions spectra look a little bit different, with some changes in relative intensities. Nevertheless, the main modes are obviously identifiable in both experiments and the following discussion will focus on them. These modes are in very good

agreement with the results of the density functional theory (DFT) calculation, Table I.

The optical phonon frequencies were studied as a function of temperature by Raman spectroscopy. Typical spectra are displayed in Fig. 1, showing the effect of thermal emission that produces a noticeable background. Up to 700 K, the bare experimental spectra are displayed, and at higher temperatures, two spectra are acquired successively with and without the laser. The latter, i.e., thermal emission, is then subtracted from the former and displayed in the bottom of Fig. 1. In this way, one can obtain satisfactory signal-to-noise ratios on the Raman lines, despite the small sample size that induces important thermal emission contribution. A fitting procedure with Bose–Einstein corrected damped harmonic oscillators was then performed, giving access to the temperature dependence of the

TABLE I. Calculated and experimental Raman modes (cm^{-1}) of α -quartz-type BPO_4 .

Mode	DFT (0 K)	Experimental (298 K)
E	1290.3	
E	1205.9	1203.1
A_1	1159.2	1165.3
A_1	1097.6	1090.6
E	1092.8	1090.6
A_2	1085.8	
E	1069.3	
A_2	1057.5	
E	947.8	
A_2	936.5	
E	929.8	
A_1	927.6	
A_2	893.3	
E	873.3	875.3
E	679.4	686.0
A_2	617.8	
E	563.9	
A_1	559.2	566.4
E	549.7	510.4
A_2	510.8	515.9
E	507.7	507.8
A_1	500.9	
E	468.5	480.3
A_1	430.7	445
A_2	401.5	
E	333.2	344.6
E	326.3	331.9
A_1	293.0	289.1
A_1	244.8	
E	234.4	
A_2	216.6	
E	187.9	187.5
E	159.4	162.0
A_2	90.3	

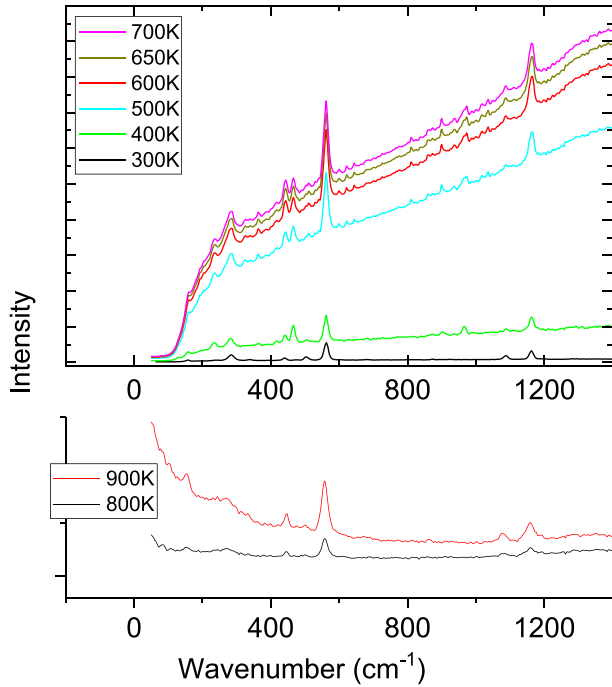


FIG. 1. Raman spectra of α -quartz BPO₄ as a function of temperature. Above: bare spectra as acquired, up to 700 K; Below: Spectra obtained after subtracting the thermal emission contribution (same measurements obtained successively, with and without the Raman laser).

wavenumber, damping, and intensity for each mode. The dependence of wavenumbers is plotted in Fig. 2, exhibiting quasiflat responses. The Grüneisen slope values $\frac{d\nu}{dT}$ fitted on these lines lie in the range of $0.001 \text{ cm}^{-1}/\text{K}$ (mean value of all slopes) and are given in the last column of Table II; these values are calculated in the range of 300–800 K since the two higher temperature point are more noisy due to the increasing thermal emission contribution.

It is interesting to compare such low values to what occurs in $\bar{1}4$ cristobalite BPO₄, so with rather similar chemical bonds, but a different crystal structure. The same experiment vs temperature was then performed (same apparatus, same data processing) on cristobalite BPO₄, and the results of the fitting procedure are given in Fig. 3. Obviously, the temperature dependence of the different lines is much higher than for those shown in Fig. 2. For a more quantitative approach, as described previously, the different mode slopes were fitted in a linear way, and they range between -0.02 and $-0.011 \text{ cm}^{-1}/\text{K}$, with a mean value of $-0.015 \text{ cm}^{-1}/\text{K}$. In the case of α -quartz BPO₄, these values range from -0.033 (mode 1090.6 cm^{-1}) to $+0.002 \text{ cm}^{-1}/\text{K}$, with a mean value of $-0.004 \text{ cm}^{-1}/\text{K}$ and four modes for which the slope lies within the estimated standard deviation (ESD). This 1090.6 cm^{-1} mode is of rather low intensity and noticeable width, and then the uncertainty on its position is quite large ($\pm 5 \text{ cm}^{-1}$). Upon removing it from the calculation, the mean value becomes $-0.0001 \text{ cm}^{-1}/\text{K}$, more than two orders of magnitude smaller than the cristobalite value.

The temperature dependence of the phonon wavenumber corresponds to the sum of an explicit [first term in Eq. (1)] and an implicit contribution [second term in Eq. (1)], which are a pure temperature

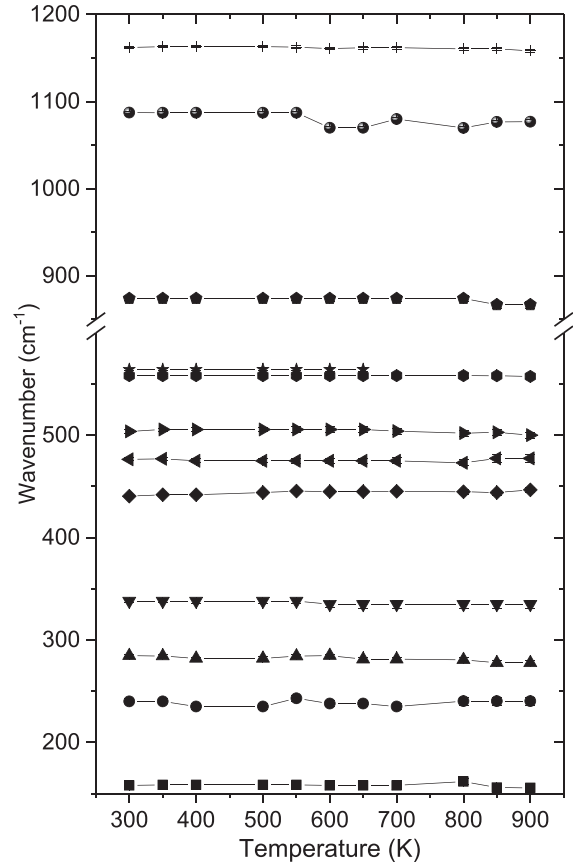


FIG. 2. Temperature dependence of the Raman modes of α -quartz BPO₄. Error bars are shown when they are larger than the symbol size.

contribution (phonon–phonon interactions) and a pure volume contribution (thermal expansion), respectively,

$$\left(\frac{d\nu_i}{dT}\right)_P = \left(\frac{d\nu_i}{dT}\right)_V + \left(\frac{\partial\nu_i}{\partial V}\right)_T \left(\frac{dV}{dT}\right)_P. \quad (1)$$

TABLE II. Raman modes (cm^{-1}) and their pressure and temperature coefficients ($\text{cm}^{-1} \text{ GPa}^{-1}$ and $\text{cm}^{-1} \text{ K}^{-1}$) for α -quartz-type BPO₄. ESDs on the last significant figure are given in parentheses. The $(d\nu/dP)_T$ values from the present first-principles calculations are given in italics in square brackets.

ν	$(d\nu/dP)_T$	$(d\nu/\nu dP)_T$	γ	$-\alpha\gamma\nu$	$(d\nu/dT)_P$
1165.3(1)	1.17(2) [0.7]	0.00100(2)	0.092(2)	-0.0042(1)	-0.004(2)
1090.6(1)	3.7(4) [3.6]	0.0034(4)	0.31(4)	-0.013(1)	-0.033(5)
875.3(1)	7.6(4) [4.7]	0.0087(4)	0.80(4)	-0.027(1)	0.000(2)
566.4(1)	4.3(1) [4.8]	0.0076(2)	0.70(2)	-0.0154(4)	0.000(2)
510.4(2)	2.8(1) [3.3]	0.0055(2)	0.50(2)	-0.0100(4)	-0.001(2)
480.3(2)	1.7(2) [1.7]	0.0035(4)	0.33(4)	-0.006(1)	-0.005(2)
445.0(1)	-0.4(1) [0.3]	-0.0009(2)	-0.08(2)	0.0010(2)	-0.009(2)
289.1(1)	9.4(2) [9.4]	0.033(1)	3.0(1)	-0.034(1)	-0.006(3)
162.0(1)	2.6(2) [2.7]	0.016(1)	1.5(1)	-0.0093(6)	0.002(2)

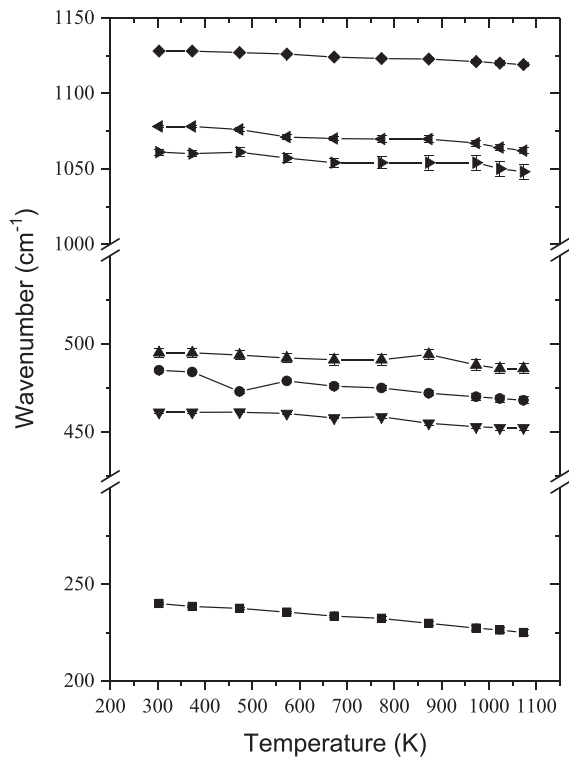


FIG. 3. Temperature dependence of the Raman modes of cristobalite BPO₄. Error bars are shown when they are larger than the symbol size.

The phonon wavenumber shift due to the latter implicit contribution of a given mode can be expressed as a function of the unit cell volume introducing the quasiharmonic mode Grüneisen parameter as follows:¹⁰

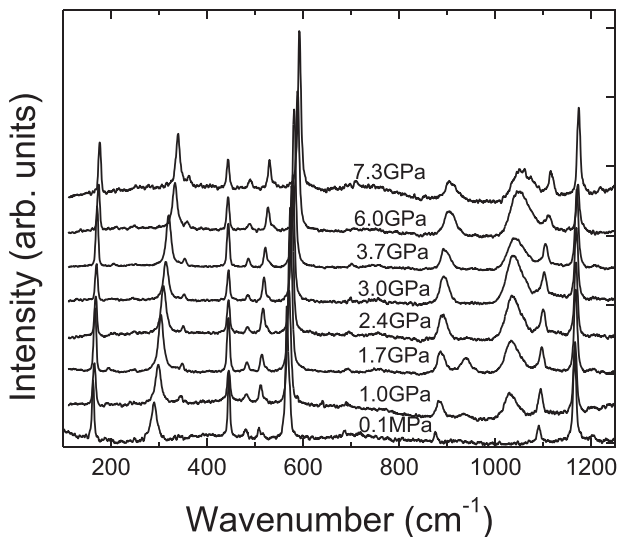


FIG. 4. Raman spectra of α -quartz BPO₄ as a function of pressure.

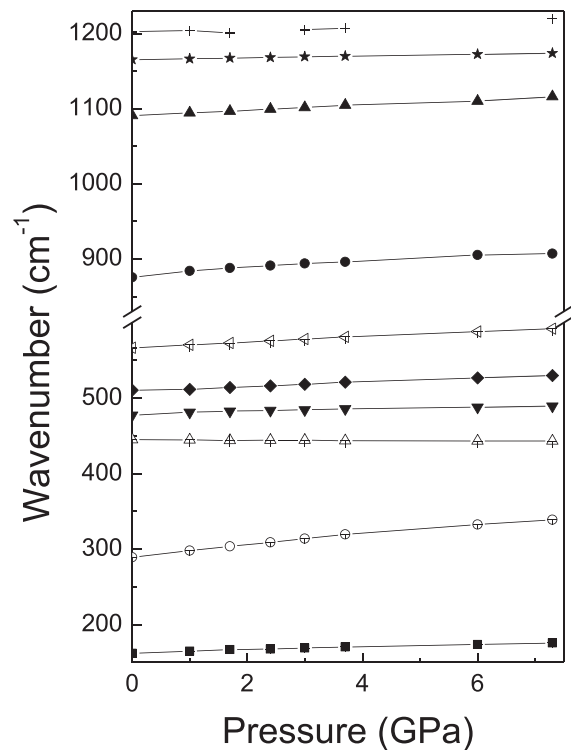


FIG. 5. Pressure dependence of the Raman modes of α -quartz BPO₄. Error bars are smaller than the symbol size.

$$\gamma_i = -\frac{d\ln\tilde{\nu}_i}{d\ln V} = -\frac{V}{\tilde{\nu}_i} \frac{d\tilde{\nu}_i}{dV}. \quad (2)$$

The implicit part of the wavenumber shift is given by the expression

$$\left(\frac{\partial\tilde{\nu}_i}{\partial V}\right)_T \left(\frac{dV}{dT}\right)_P = -\alpha\gamma_i\tilde{\nu}_i. \quad (3)$$

Nine modes were investigated as a function of pressure, Table II. The pressure shifts of these modes do not exhibit any anomalous behavior (Figs. 4 and 5) and are comparable to those of other α -quartz-type phosphates.^{17–19} This is confirmed by the pressure shifts determined from the DFT calculations, which are in very good qualitative and, in most cases, quantitative agreement with the experimental values. The present results allowed the quasiharmonic mode Grüneisen parameter and the implicit contributions to the wavenumber shift to be obtained for each mode using experimental values of α , the thermal expansion coefficient ($3.9 \times 10^{-5} \text{ K}^{-1}$), and the volumes readily obtained from the bulk modulus (92 GPa).⁴ The latter is essentially identical to the 91 GPa obtained from the present DFT calculations, indicating that the theoretical elastic behavior is fully consistent with the bulk modulus obtained from *in situ* structural analysis under pressure.⁴ It is clear that the quasiharmonic mode Grüneisen parameters exhibit quite usual values and that the behavior as a function of temperature arises from compensation of the implicit contribution from thermal expansion calculated here by anharmonic effects. In particular, for seven out of the nine modes followed, the explicit and implicit contributions will

have opposite signs. The ultrastable optical phonon frequencies as a function of temperature arising from a compensation between phonon-phonon interactions and implicit contributions due to thermal expansion in α -quartz BPO₄ are entirely consistent with the absence of any instability and any high-temperature phase transitions to β -quartz or cristobalite-type forms up to the sublimation of α -quartz BPO₄ at close to 1100 K (Ref. 4). This absence of any structural instability may be an indication that the acoustic phonons are also stable. The compensation, as found in the present material giving rise to stable phonon frequencies, is very unusual and has been observed very rarely, for example, in body-centered cubic metals such as vanadium,²⁰ which only possess acoustic phonons. In another material UO₂ (Ref. 21), the frequencies of the higher-energy optical phonons exhibit strong temperature stability due to similar compensation; however, lower-energy optical and the acoustic phonons exhibit softening.

The present results indicate that BPO₄ could exhibit very stable piezoelectric properties at high temperature. This could be of great interest for applications as oscillators in space and those at high-temperature such as microbalances, pressure sensors, and field test viscometers, which in the case of α -quartz are limited to a maximum of 846 K due to the transition to the β phase²² or require cooling systems to limit the variation in the piezoelectric response and to avoid this phase transition.

REFERENCES

- ¹F. Dachille and L. S. D. Glasser, *Acta Crystallogr.* **12**, 820 (1959).
- ²K. Kosten and H. Arnold, *Z. Kristallogr.* **152**, 119 (1980).
- ³J. Haines, O. Cambon, R. Astier, P. Fertey, and C. Chateau, *Z. Kristallogr.* **219**, 32 (2004).
- ⁴J. Haines and O. Cambon, *Z. Kristallogr.* **219**, 314 (2004).
- ⁵R. J. Angel, D. R. Allan, R. Milletich, and L. W. Finger, *J. Appl. Crystallogr.* **30**, 461 (1997).
- ⁶J. Kalus, B. Dorner, V. K. Jindal, N. Karl, I. Natkaniec, G. S. Pawley, W. Press, and E. F. Sheka, *J. Phys. C: Solid State Phys.* **15**, 6533 (1982).
- ⁷V. K. Jindal and J. Kalus, *J. Phys. C: Solid State Phys.* **16**, 3061 (1983).
- ⁸F. Cerdeira, F. E. A. Melo, and V. Lemos, *Phys. Rev. B* **27**, 7716 (1983).
- ⁹W. Hafner and W. Kiefer, *J. Chem. Phys.* **86**, 4582 (1987).
- ¹⁰R. Ouillon, J.-P. Pinan-Lucarre, and P. Ranson, *J. Raman Spectrosc.* **31**, 605 (2000).
- ¹¹I. Gregora, N. Magneron, P. Simon, Y. Luspain, N. Raimboux, and E. Philippot, *J. Phys. Condens. Matter* **15**, 4487 (2003).
- ¹²H. K. Mao, J. Xu, and P. M. Bell, *J. Geophys. Res.* **91**(B5), 4673, <https://doi.org/10.1029/JB091iB05p04673> (1986).
- ¹³J. P. Perdew and Y. Wang, *Phys. Rev. B* **45**, 13244–13249 (1992).
- ¹⁴X. Gonze, B. Amadon, P. M. Anglade, J. M. Beuken, F. Bottin, P. Boulanger, F. Bruneval, D. Caliste, R. Caracas, M. Côté *et al.*, *Comput. Phys. Commun.* **180**, 2582–2615 (2009).
- ¹⁵H. J. Monkhorst and J. D. Pack, *Phys. Rev. B* **13**, 5188–5192 (1976).
- ¹⁶P. Hermet, L. Gourrier, J.-L. Bantignies, D. Ravot, T. Michel, S. Deabate, P. Boulet, and F. Henn, *Phys. Rev. B* **84**, 235211 (2011).
- ¹⁷A. Jayaraman, D. L. Wood, and R. G. Maines, Sr., *Phys. Rev. B* **35**, 8316 (1987).
- ¹⁸M. J. Peters, M. Grimsditch, and A. Polian, *Solid State Commun.* **114**, 335 (2000).
- ¹⁹E. Angot, B. Huang, C. Levelut, R. Le Parc, P. Hermet, A. S. Pereira, G. Aquilanti, G. Frapper, O. Cambon, and J. Haines, *Phys. Rev. Mater.* **1**, 033607 (2017).
- ²⁰P. D. Bogdanoff, B. Fultz, J. L. Robertson, and L. Crow, *Phys. Rev. B* **65**, 014303 (2001).
- ²¹M. S. Bryan, J. W. L. Pang, B. C. Larson, A. Chernatynskiy, D. L. Abernathy, K. Gofryk, and M. E. Manley, *Phys. Rev. Mater.* **3**, 065405 (2019).
- ²²R. A. Young, Report No. AD 276 235 (Defence Documentation Centre, Washington, DC, 1962).